Optics and Lasers in Engineering 50 (2012) 29–38

Contents lists available at ScienceDirect

Optics and Lasers in Engineering

journal homepage: www.elsevier.com/locate/optlaseng

Reconstruction of the density field using the Colored Background Oriented Schlieren Technique (CBOS)

F. Sourgen, F. Leopold *, D. Klatt

French-German Research Institute of Saint-Louis (ISL), 5 rue du Général Cassagnou, 68300 Saint-Louis, France

ARTICLE INFO

Available online 19 August 2011

Keywords:
Compressible flow
Reconstruction
Schlieren technique
Three-dimensional flow

ABSTRACT

In this paper the improved Background Oriented Schlieren technique called CBOS (Colored Background Oriented Schlieren) is described and used to reconstruct density fields of three-dimensional flows. The Background Oriented Schlieren technique (BOS) allows to measure the light deflection caused by density gradients in a compressible flow. For this purpose the local image displacements of the image of a background pattern observed through the flow is used. In order to increase the performance of the conventional Background Oriented Schlieren technique, the monochromatic background is replaced by a colored dot pattern. The different colors are treated separately using suitable correlation algorithms. Therefore, the accuracy and the spatial resolution can be increased. A tomographic reconstruction method is then used to reconstruct the density field in three-dimensional flows from CBOS measurements.

1. Introduction

For the investigation of compressible flows the determination of the density distribution is of prime importance. For this purpose, the schlieren method, introduced by A. Toepler in 1864, is currently used [1]. The schlieren technique transforms the phase variation of the light passing through a phase object into an intensity variation. In the review paper by Desse and Deron [2] an overview of the different Schlieren, interferometric and holographic techniques is given. Other techniques such as the density speckle photography appeared in the seventies and allow to measure directly the deflection of the light [3,4]. Later, Wernekink and Merzkirch [5], Niessen et al. [6] have used an improved version of the density speckle photography for this purpose.

The Background Oriented Schlieren technique is based on a patent held by Meier [7] and more precisely described by Raffel [8]. In order to measure the light deflection caused by density gradients in a compressible flow, the BOS technique uses the local image displacements of a background image. Tiny, randomly distributed dots on a flat plate are used as a background. The recording has to be performed as follows: firstly a reference image is generated by recording the background pattern observed through the air at rest before or after the experiment. Secondly, an additional exposure through the flow under investigation leads to a displaced image of the background pattern. The resulting images of both exposures can then be evaluated by correlation methods, leading to the local displacements, thus to the deviations of the rays. This paper describes how to improve the accuracy and spatial resolution of the BOS technique using a background pattern of colored dots and suitable correlation algorithms (CBOS technique).

Furthermore, the deviations of the rays in a given observation direction are a projection of the (gradient of) density field in the flow. Indeed a tomography reconstruction method is used to reconstruct the density field in various compressible flows. This paper also describes the tomographic technique and the reconstruction results.

2. Background Oriented Schlieren technique

2.1. Principles of the BOS technique

The principle of the BOS technique is based on the measurement of the deviation of the light passing through a phase object. Indeed the BOS technique uses the local image displacements of a background image for detecting the changes in density gradients. Thanks to the empirical law of Gladstone–Dale G, the density can directly be related to the refractive index:

$$\frac{n-1}{\rho} = G(\lambda) \quad \text{with}$$

$$G(\lambda) = 2.2244 \times 10^{-4} \frac{\mathrm{m}^3}{\mathrm{kg}} \left(1 + \left(\frac{6.7132 \times 10^{-8}\mathrm{m}}{\lambda}\right)^2 + \left(\frac{1.0686 \times 10^{-7}\mathrm{m}}{\lambda}\right)^4\right), \quad (1)$$

* Corresponding author. Tel.: +33 389 69 50 61.
E-mail address: friedrich.leopold@isl.eu (F. Leopold).

0143-8166/$ - see front matter © 2011 Elsevier Ltd. All rights reserved.
doi:10.1016/j.optlaseng.2011.07.012

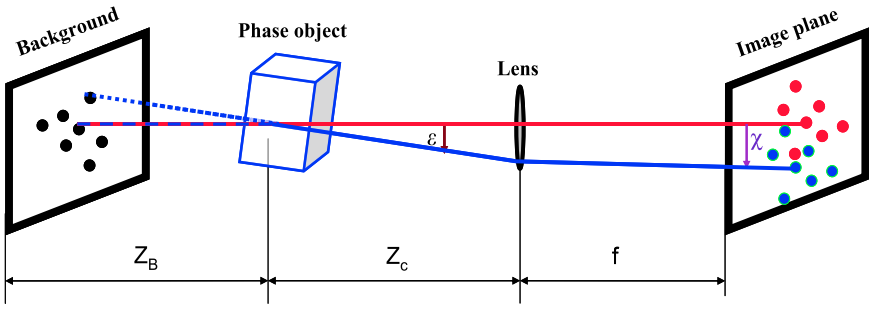

Fig. 1. Optical setup for the BOS technique.

where n denotes the refractive index, which is defined as the ratio of the speed of light in vacuum to the speed of light in the optical medium; ρ replaces the density of the medium, G denotes the Gladstone–Dale constant, which depends on the characteristics of the gas and λ represents the wavelength of the light. As the changes in the Gladstone–Dale constant in the visible spectral range are very small, the constant is set at the value $G(\bar{\lambda}) = 2.26 \times 10^{-4}\,\mathrm{m^3/kg}$ for an average wavelength of $\bar{\lambda} \approx 550\,\mathrm{nm}$.

The local image displacement χ can be expressed by integrating the local index gradients along the light path:

$$\chi = \frac{fZ_B}{Z_C + Z_B - f} \int_{\Delta_z} \frac{1}{n_0} \frac{\delta n}{\delta r(x,y)} dz, \tag{2}$$

where z represents the coordinate along the light path, f the focal length of the camera lens, Z_C the distance from the camera to the phase object and Z_B the distance from the phase object to the background image, as shown in Fig. 1. Now the Gladstone–Dale relation allows us to draw conclusions from the two-dimensional local image displacements $\chi(x,y)$ in order to determine the density gradients $\delta\rho/\delta x$ and $\delta\rho/\delta y$ in the horizontal and the vertical directions, respectively [9,10].

2.2. The color distribution in the background image

The CBOS technique normally uses a computer-generated random dot pattern, which is placed in the background of the test volume. This pattern has to possess a high spatial frequency that can be imaged with a high contrast. It usually consists of tiny, randomly distributed dots. Earlier studies [11] pointed out that the dot pattern for an optimized evaluation should cover from 30% to 70% of the surface of the background image.

Since the primary colors red, green and blue (according to the RGB color model) can easily be detected by commercial digital CMOS cameras, these colors are used to generate the colored background for the CBOS technique. The background pattern is assembled as follows: the same proportion of each primary color is distributed randomly over the background image. This leads to a specific distribution of pure and compound colors over the background (Fig. 2). It can be observed that a filling rate of 35% for each primary color leads to a maximum distribution of the pure colors. Furthermore, the distribution of the compound colors and of the uncolored areas is close to 30%. A typical colored background image is shown in Fig. 3 with a filling rate of 35% for each primary color.

2.3. Image processing

In order to improve analysis of the recorded images, the post processing takes into account that digital CMOS cameras have sensors for the primary colors red, green and blue. In order to assume valuable color detection by the camera the image of the dots on the CCD sensor should at least cover 2×2 pixels. The data from the sensors are directly stored without any treatment or compression, using a special raw format. All pixels fulfilling the threshold criteria for the red, green or blue color are added to the corresponding dot pattern. Due to the decomposition into

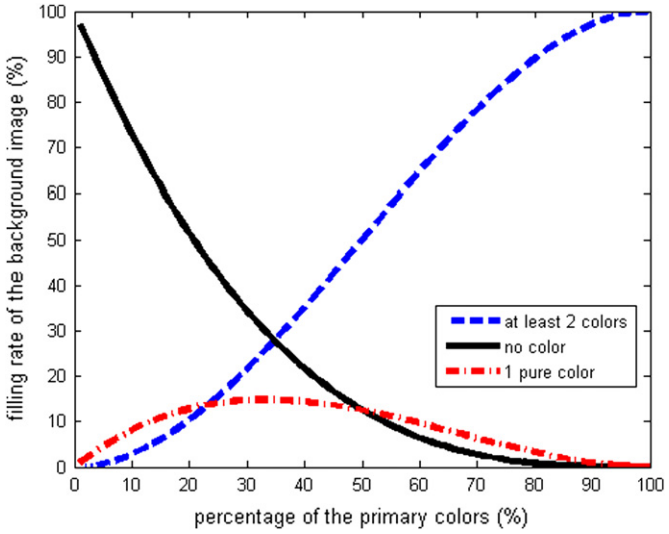

Fig. 2. Distribution of the compound colors as a function of the primary color filling rate.

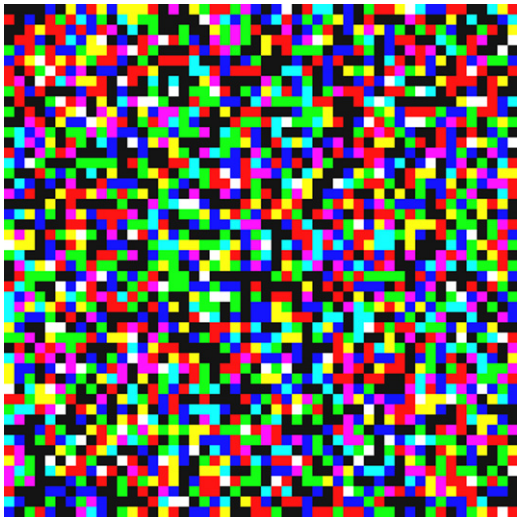

Fig. 3. Colored background image.

the three primary colors, 8 elementary dot patterns can be extracted from the image (Fig. 4):

- one pattern for each of the primary colors (red, green and blue),
- one pattern for all secondary colors,
- 3 patterns of dots containing red, green and blue color and
- one pattern for the uncolored areas, the so-called "black dots".

The assessment of the image local image displacements is achieved by treating each of the 8 elementary patterns separately using the cross-correlation method already applied in the PIV technique [12–15]. In order to increase the accuracy of the common BOS technique, a gliding interrogation window is employed. Therefore the interrogation windows for the different dot patterns are not treated at the same place. Instead all the dot patterns are treated simultaneously. The interrogation windows are shifted by one-eighth of its length and for different dot patterns (Fig. 5) in such a manner that at the end, every interrogation window is surrounded by the results of the other dot patterns. The size of the interrogation windows for the following test cases is 32×32 pixels. At last an average value for each location is determined by the value obtained at the location itself and by the results from interpolations between the opposite neighboring values (Fig. 6). In order to increase the accuracy of the measurement, the values used for the averaging must satisfy a standard deviation criterion. A more detailed description and a comparison between the BOS and the CBOS technique can be found in Leopold et al. [11].

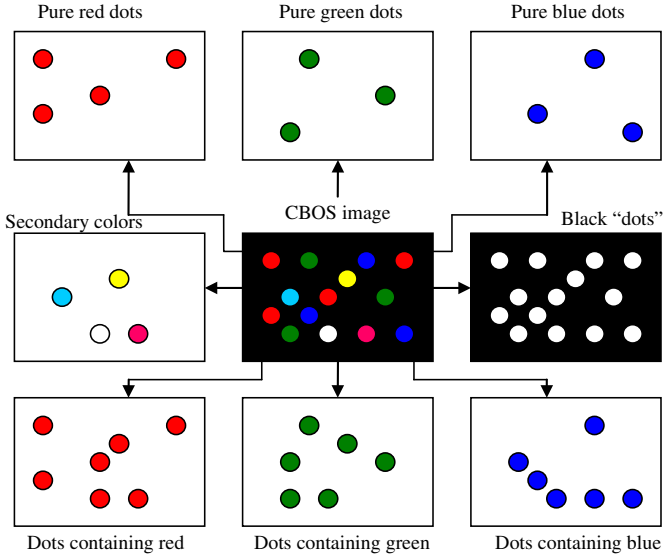

Fig. 4. Extraction of the 8 elementary dot patterns from the colored background image.

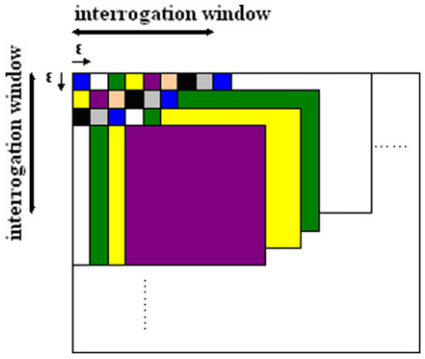

Fig. 5. Gliding interrogation windows.

3. Reconstruction

The reconstruction of the density field from CBOS measurement depends if the flow is axis symmetrical or three-dimensional. If the

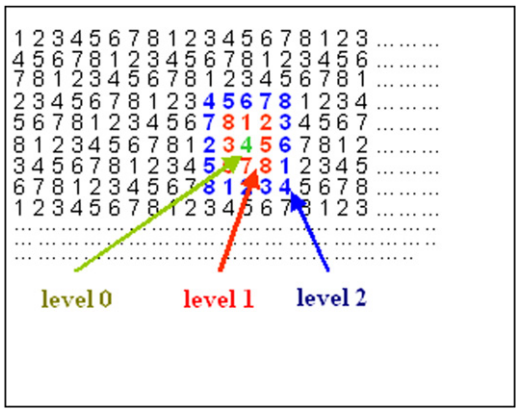

Fig. 6. Neighboring points taken into account for the averaging (numbers 1 to 8 indicate the different dot patterns).

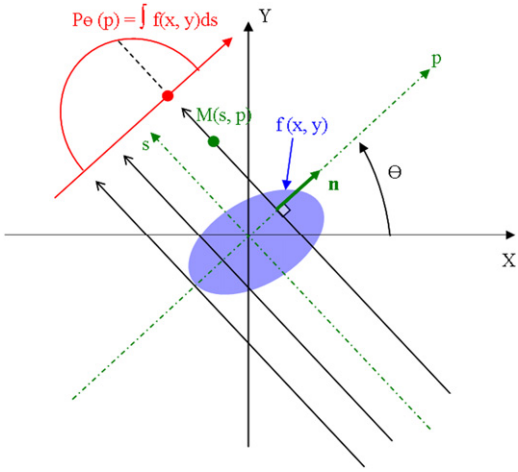

Fig. 7. Radon transformation.

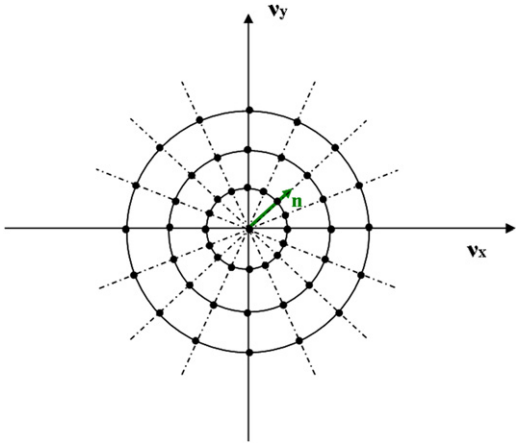

Fig. 8. Fourier slice theorem.

flow can be considered as axis symmetrical in good approximation, reconstruction algorithms based on the Abel or Radon transformation might be used. In particular, the direct Abel transformation or the filtered backprojection algorithm can attractively be used to obtain reliable results (Meier 2004, [15,16]).

However, in the case of asymmetric flows and in the case of incomplete projections, such as the flow around a body with incidence, the reconstruction technique encounters the problem of the limited number of projections and also the discontinuity of these projections, possibly masked by the body. It has to be noticed that the discontinuity of the projections becomes a problem only in the case of asymmetric flows. Indeed, in the case of axis symmetrical flows there is no angular discontinuity in the sinograph (angular representation of the projections) because the contour lines follow the body shape (circles). But in the case of asymmetric flows, the mask due to the body interrupts the projections' contour lines so that we call it "incomplete projections". Then a filter can be used for the masked part of the projections, except if the discontinuity is too much important because the filter has to link incomplete projections on both sides.

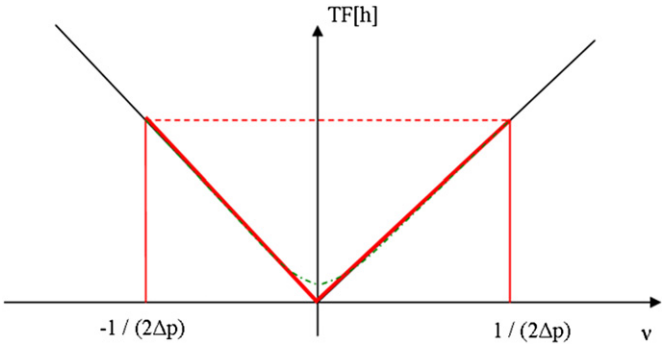

Fig. 9. Ramp filter.

Indeed, in the case of asymmetric fields, the easy-to-use filtered backprojection algorithm is considerably impacted by the numerical artifacts related to the limited number of, possibly incomplete, projections. Then the literature suggests other kinds of algorithms [17]. However, in the particular case of the density field of a compressible flow, we propose to conserve the filtered backprojection algorithm approach, but we have to investigate and to correct the main numerical artifacts encountered.

3.1. *The filtered backprojection algorithm*

In this section the filtered backprojection algorithm strategy is quickly reminded. Particularly complete and interesting developments can be found in Kak and Slaney [18] and in Grangeat [17] for instance. The filtered backprojection algorithm is an analytical approach based on the Radon transformation for parallel rays, the Fourier slice theorem and the convolution theorem.

Firstly the measurement of projections is described using the Radon transformation operator, as illustrated in Fig. 7. In this

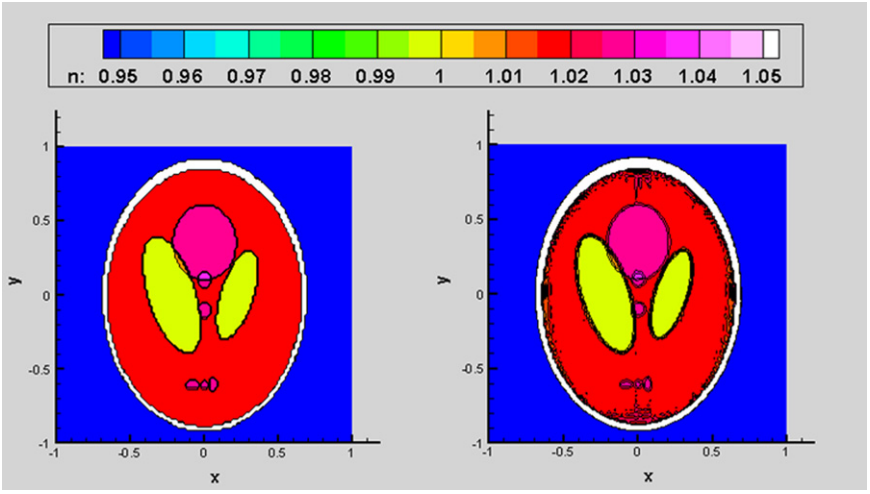

Fig. 10. Shepp and Logan "Head phantom" type of field (left) and reconstruction (right, from 100 projections).

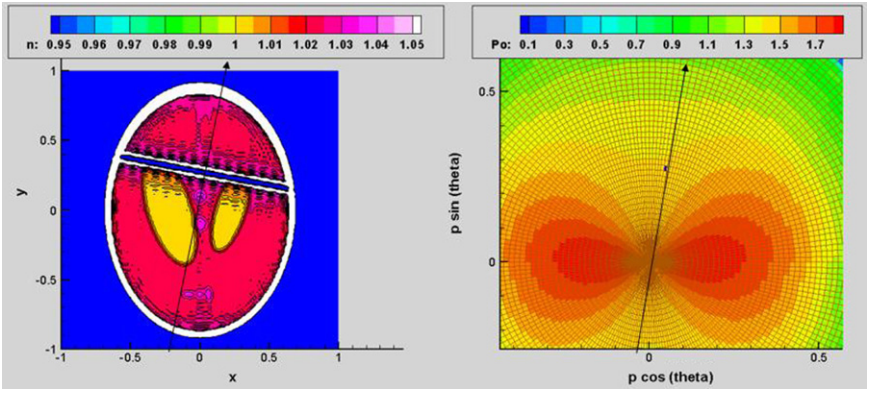

Fig. 11. Reconstruction from incomplete projections (one single pixel is masked).

formalism, the measurement of projections in a given slice is the Radon transformation of the scalar field "f" to be determined as follows:

$$\mathbf{R}[f](\theta,p) = P_\theta(p) = \int_{rayp} f(x,y)ds$$

The Fourier slice theorem then allows writing the one-dimensional Fourier transformation of the projections using the bidimensionnal Fourier of the field to be reconstructed (Fig. 8):

$$\mathbf{TF_p}(\mathbf{R}[f])(\theta,v) = \mathrm{TF}(f)(v\cos\theta, v\sin\theta) = \mathrm{TF}(f)(v\vec{\mathbf{n}})$$

A consequence of the invariance by translation and of the Fourier slice theorem is the convolution theorem, which allows determining the scalar field f:

$$\mathbf{R}^+[h_p^* \mathbf{R}[f]] = \mathbf{R}^+[h]^* f$$

R+ is the adjoint operator and h is a one-dimensional function. To determine the scalar field f, the function h has to be chosen such as the adjoint operator applied to h gives the Dirac function. The solution is given by the convolution kernel $\mathrm{TF}[h] = |\upsilon|$. Then the Fourier transformation of the function h is a ramp function and the function h is the so-called the ramp filter (Fig. 9). Therefore the reconstruction of the scalar field f consists of backprojecting the filtered projections.

The filter h is indeed the combination of the derivative operator and of the Hilbert transformation multiplied by the factor $1/2\Pi$. Moreover, as the support of h is not confined, it has to be multiplied by a low-pass filter (Hamming window for instance) with a maximum frequency compatible with the Nyquist criterion.

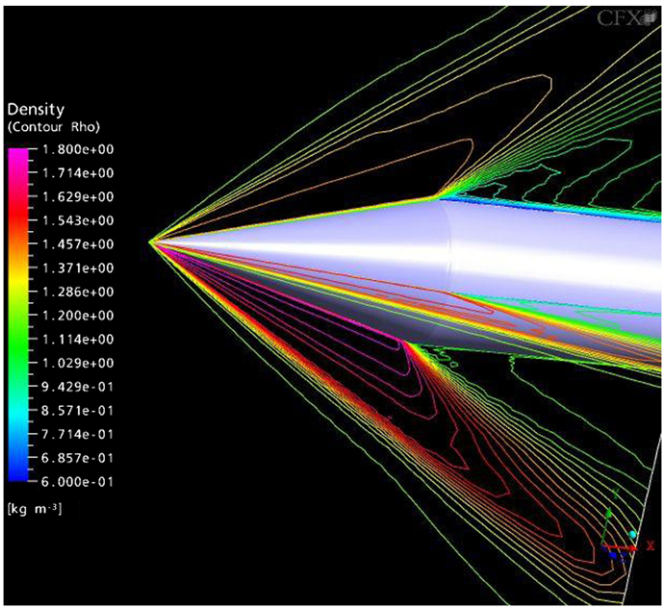

Fig. 14. RANS simulation of the flow around a cone (14° half angle) at 6° angle of attack (Mach number 2).

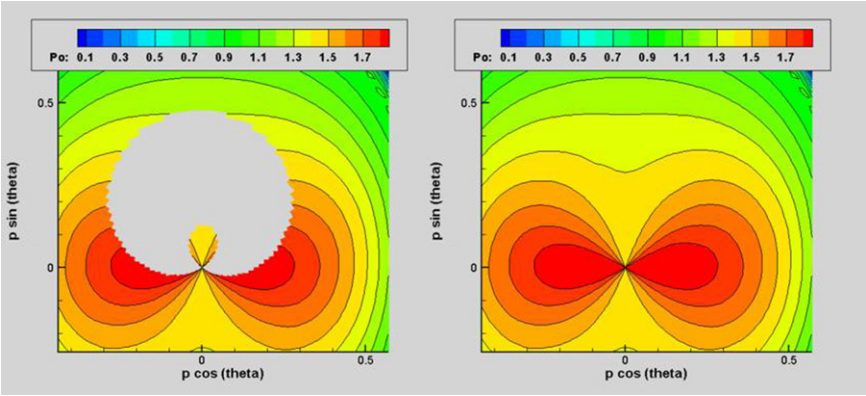

Fig. 12. Incomplete projections and interpolated projections.

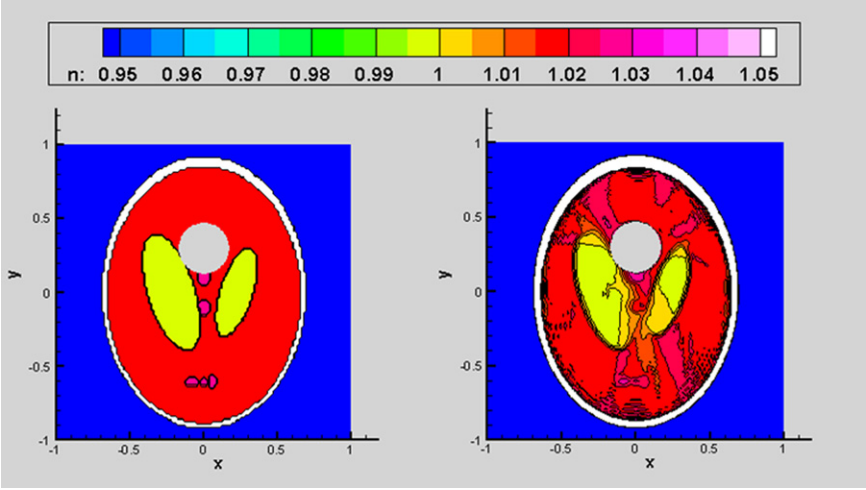

Fig. 13. Original field (with "opaque" body) and reconstruction from interpolated projections.

In order to assess the accuracy of reconstruction algorithms in X-ray tomography, for medical purposes, the Shepp and Logan "head phantom" is often used because the human head is believed to be extremely demanding on the numerical accuracy [19]. The phantom, shown in Fig. 10, is a superposition of 10 ellipses, which divide the refractive index field in local regions of constant value. It might seem surprising to use such a case in testing the ability of the CBOS technique to reconstruct cross sections of supersonic flows, and yet, the weak point of the correlation-based BOS methods in supersonic flows is the crossing of shock waves by rays, which generates astigmatism and locally blurred images due to strong steps of refractive index, what the phantom exactly consists of (Sourgen et al., [15]). Furthermore, the parallel projections through the phantom field can be generated analytically, so very quickly. In addition, the central ellipse of the phantom field can be easily masked to "simulate" a model standing in the flow and to investigate the reconstruction from incomplete projections. This is a preliminary but important work for testing the reconstruction algorithms, more accurate investigations are detailed afterwards. An example of the analytical reconstruction using the filtered backprojection algorithm from 100 projections is shown in Fig. 10.

3.2. Numerical test cases

The numerical artifacts related to a discontinuity in the projections are illustrated by Fig. 11. When a single pixel is masked (value equaled to zero) in the sinograph, the reconstruction is strongly damaged along the direction perpendicular to the projection, because of the discontinuity in the projections contour lines. In the case of a large lack of information (body in a wind tunnel for instance), the discontinuity of the masked part of the projections has to be filtered or the projections have to be interpolated. Whatever the interpolation, the reconstruction around the body should remain, in theory, the same. However, as any discontinuity produces numerical artifacts, an interpolation by continuity of the first derivative at least is needed in the masked part of the sinograph. Such an interpolation is shown in Fig. 12. Fig. 13 shows that the reconstruction of the refractive index is then improved.

In order to validate the approach and to estimate the reconstruction errors for realistic density fields and realistic number of projections, some numerical simulations of the flow, projections and reconstruction are performed in the case of the flow around a cone-cylinder body at Mach number 2° and at 6° angle of attack. The simulation of the flow itself is performed using a steady

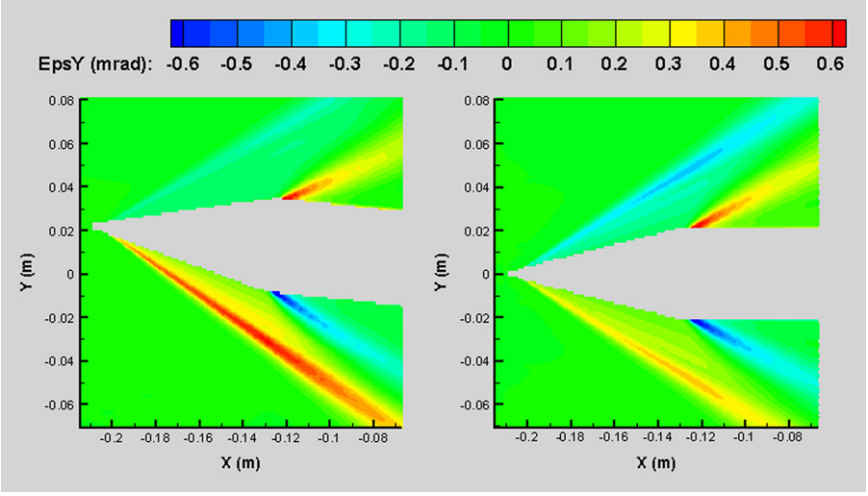

Fig. 15. Ray trajectory computation of the projections (deviations of the rays) along the directions 0° and 90°.

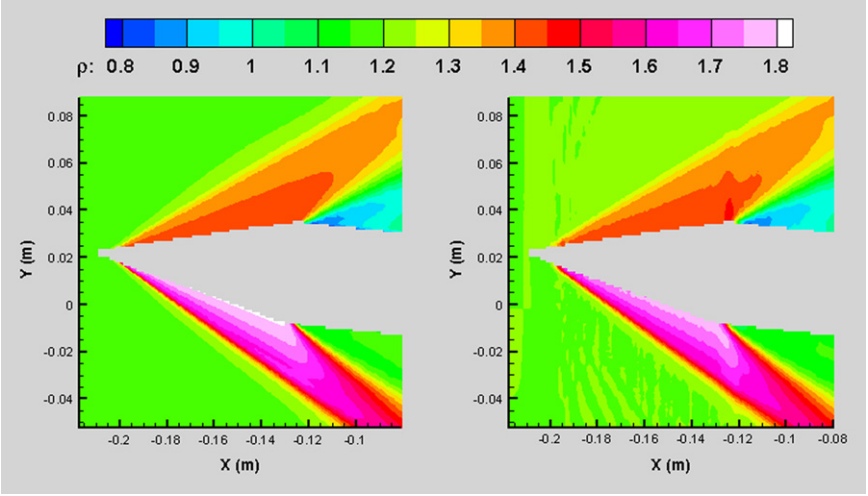

Fig. 16. Initial density field (left) and reconstruction (right, from 19 projections) in the vertical plane.

Reynolds Averaged Navier Stokes equations (RANS) approach and the ANSYS CFX tool (Fig. 14). The quality of the simulation (grid and parameters) is not of prime importance here, the important point is that the CBOS measurements are simulated from this numerical flowfield using a ray trajectory computation along 19 directions, from 0° to 90°, every 5°. A limited number of realistic and incomplete projections are thus obtained (Fig. 15). Then, the above-mentioned algorithms are used to reconstruct the initial numerical density field, as shown in Fig. 16.

In Fig. 17 it can be observed that the reconstruction error, defined as the relative error between the initial flowfield and the reconstructed field, remains lower than a few percentages in the most part of the flow.

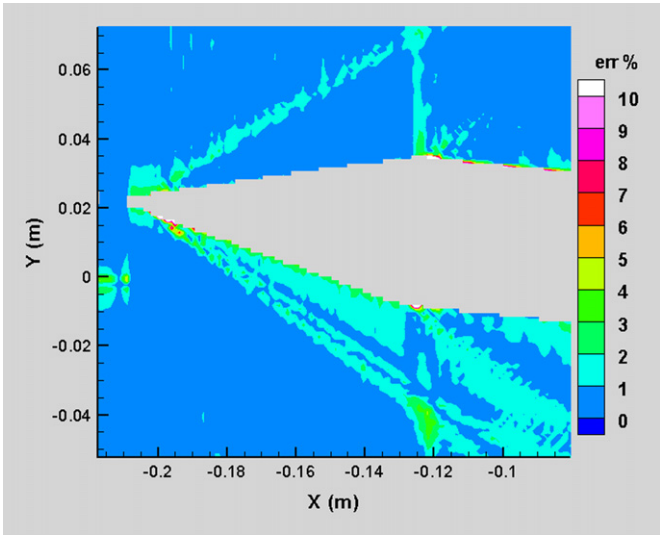

Fig. 17. (Relative) Reconstruction error in the vertical plane.

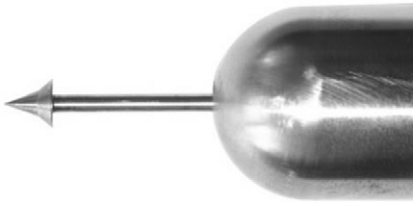

Fig. 18. Spike-tipped body.

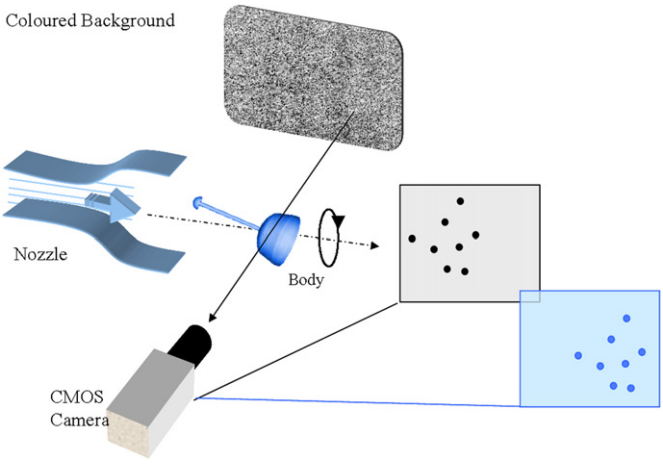

Fig. 19. Experimental apparatus.

4. Test cases

4.1. Wind-tunnel tests

The experiments are carried out in the 0.2 m × 0.2 m supersonic blow-down wind tunnel of ISL with freestream Mach numbers of 2 and 3. The Reynolds number Re_D based on the model diameter (D=40 mm) is 2.1×10^6 and 2.7×10^6; the tunnel freestream static pressure p is 575 hPa and 190 hPa. The test models used for this investigation have a cylindrical centerbody mounted on a sting assembly along the wind-tunnel centerline. For Mach number 2, the nose is a cone (14° half-angle) and for Mach number 3 it is a spike-tipped body equipped with a biconical tip (Fig. 18).

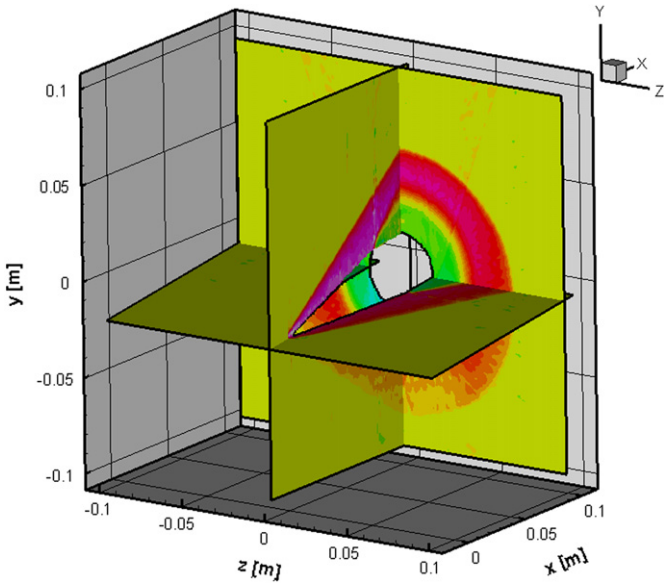

Fig. 20. 3D reconstruction of the flow around a cone-cylinder body from CBOS measurements (Mach number 2, AoA −6°).

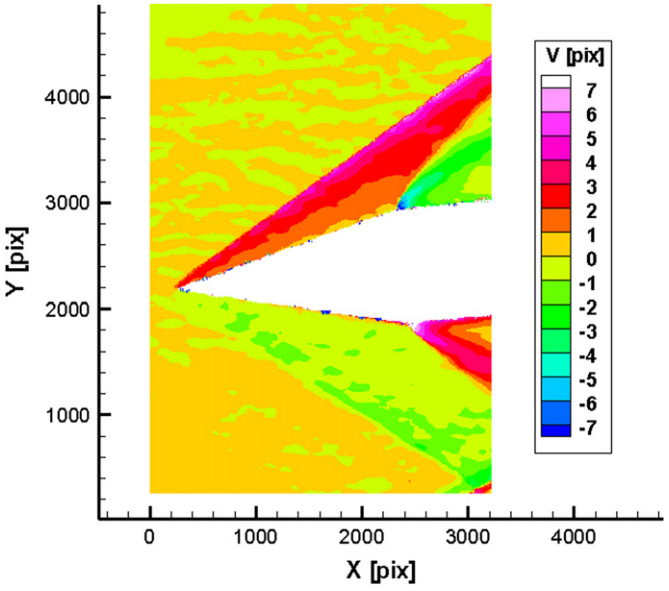

Fig. 21. Vertical displacement (projection 0°).

In order to measure projections along different directions the support of the body can be rotated every 5° around the upstream flow direction. Obviously the center of rotation remains at the same location. The experimental apparatus is shown in Fig. 19.

The CBOS images are recorded with a high-resolution camera (Canon EOS 1 Ds Mark II) equipped with a suitable telephoto lens (f=400 mm). The camera is focused on the artificial background. In order to increase the depth of the field, all pictures are taken with the smallest aperture (1/64). The camera has a CMOS sensor with a resolution of 4992×3328 pixels and the correlation windows used are 40 pixels wide. The distance Z_B between the background and the model is set at 600 mm, the distance Z_C between the model and the lens of the camera is equal to 1400 mm. The background is illuminated by a flashlamp for a duration of 2.5 μs.

The quality of the technique, particularly the spatial resolution, can be appreciated for both of the cases in Figs. 21 and 25.

One projection is recorded during one blow down. The total number of projections is hence 19. Indeed, several recordings are made during each blow down, so that each projection is the mean value of these instantaneous recordings.

In the case of the cone-cylinder (Figs. 20–22), the reconstruction of the flowfield is rather close to a RANS numerical simulation. However, the density seems to be somewhat underestimated in the lower part of the vertical plane, where the gradients are weak. The reason is that the supersonic flow is not exactly steady in the wind tunnel, because of the successive turbulent structures streaming along the flow direction. These structures are smoothed using multiple recordings and using a longer exposure time. But the latter makes the signal over noise ratio (SNR) to

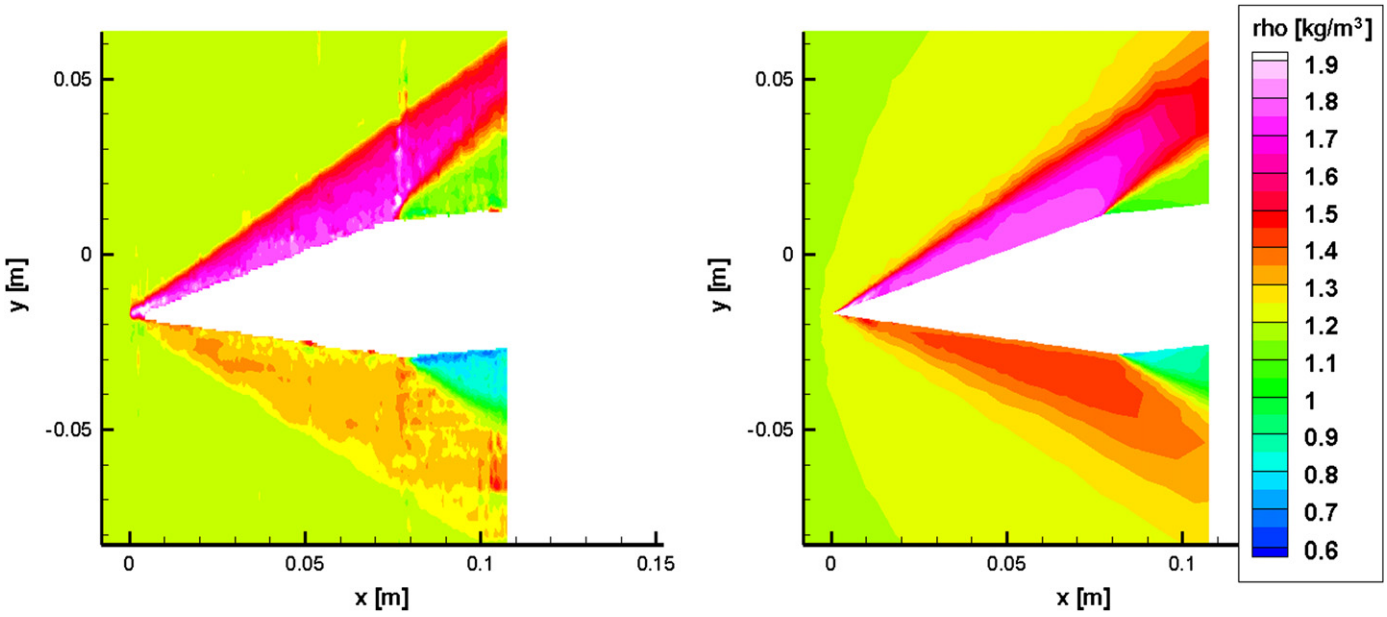

Fig. 22. Comparison between reconstruction (left) and RANS simulation (right) in the vertical plane.

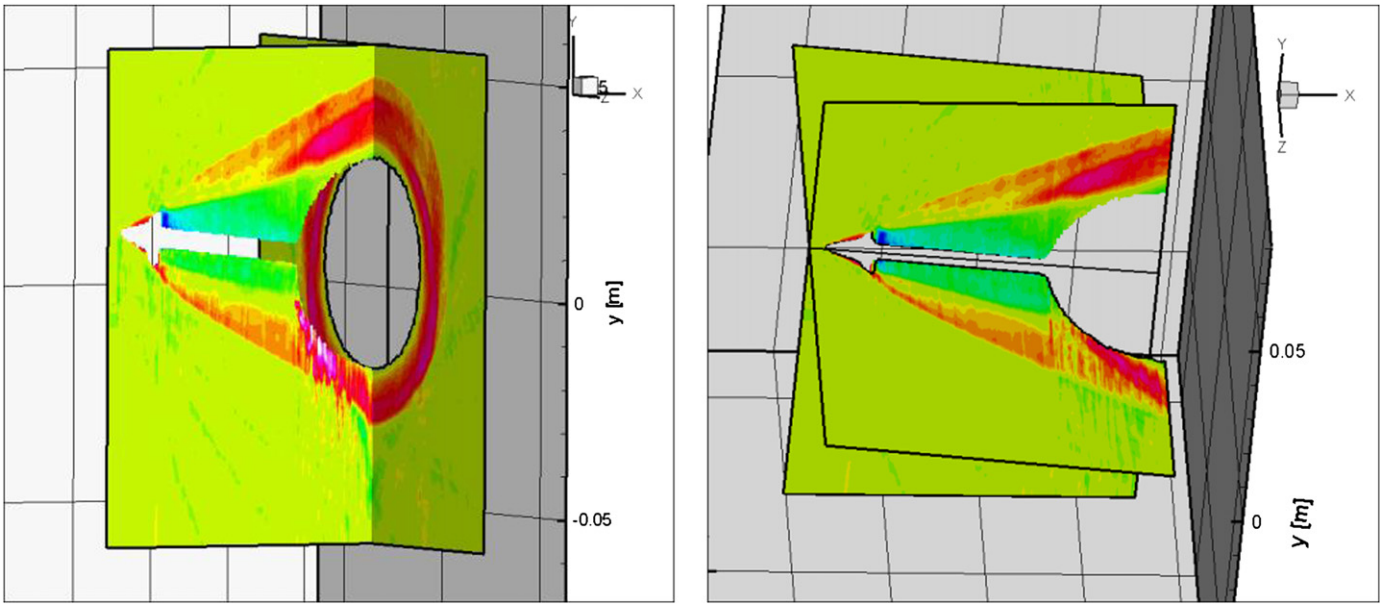

Fig. 23. Reconstruction from CBOS measurements of the density field in the flow around a spike-tipped body (Mach number 2, AoA 6°, 19 projections).

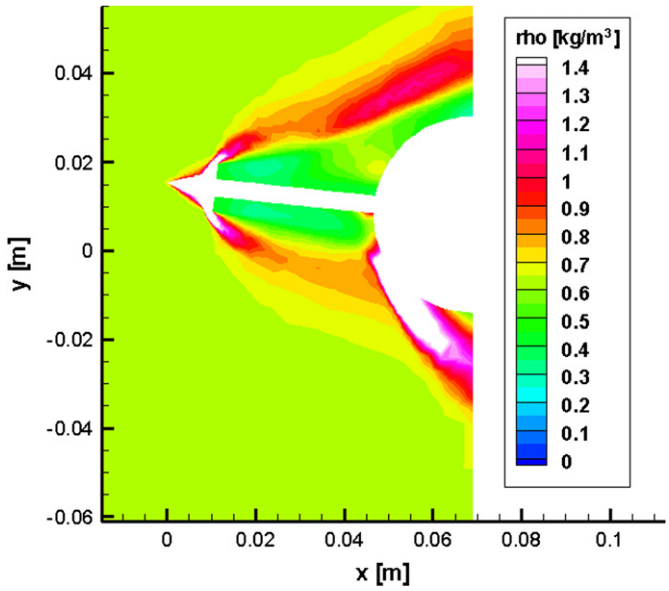

Fig. 24. (coarse grid) RANS simulation.

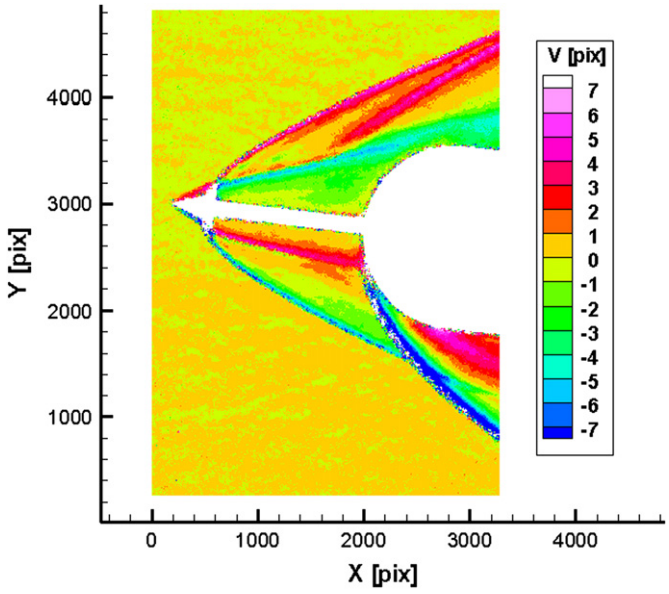

Fig. 25. CBOS vertical displacement (projection 0°).

decrease. In the upper part of the cone, the quality of the measurement remains rather good because the gradients are strong, but in the lower part, where the gradients are weaker, it can be observed in Fig. 21 that the contour lines of the projections are of lower quality due to the SNR decrease.

In the case of the flow around the spike-tipped body, a good reconstruction of the recirculating zone and of the upper shock is obtained (Fig. 23). However, at the tip and in the strong compression shock in the lower part, the value of density is underestimated. This is related to the astigmatism problems encountered by all the (C)BOS techniques in the case of very strong density gradients [15]. In such regions, the deviations are underestimated, indeed not measured at all, so that the reconstruction is strongly distorted in these regions Fig. 24.

4.2. *Free-flight test*

The investigations are based on the flow around a model of a space vehicle (European Spatial Agency ESA) with a diameter $D=92$ mm and a length $L=50.75$ mm (Fig. 26). The model is accelerated with a normal powder gun (caliber: 100 mm). The location for the measurements is at a distance of 15 m from the muzzle of the cannon. In that position the actual velocity of the model is 555 m/s, which corresponds to a Mach number of 1.63. Again the digital camera (Canon EOS 1Ds Mark II) equipped with a telephoto lens ($f=400$ mm) is used. As already mentioned, the pictures are taken with the smallest aperture (1/64). The distance Z_B between the background and the model is 417 mm and the distance Z_C between the model and the lens of the camera is 2345 mm. The colored dot patterns are printed on a transparent background (dimensions of 410×630 mm^2), which is illuminated from behind by a flashlamp. The flash lasts for 2 μs.

Due to the low Mach number 1.63, the bow shock is particularly detached from the body. The shedding vortices from the base can be seen in the representation of the horizontal displacement (Fig. 27).

A density reconstruction is obtained from the CBOS measurements and is shown in Fig. 28. In the detached shock region near the nose, the density gradients are so strong that the quality of the measurements does not allow a reliable reconstruction, but in the wake region a good reconstruction of the density field is obtained.

5. Conclusions

The Background Oriented Schlieren technique is a promising tool for the three-dimensional analysis of a flow with density gradients.

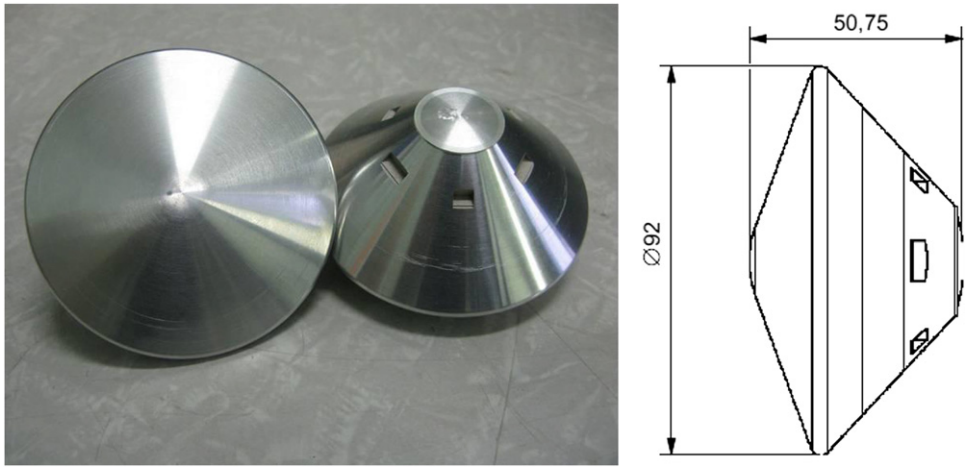

Fig. 26. Model of the space vehicle (photography and dimensions).

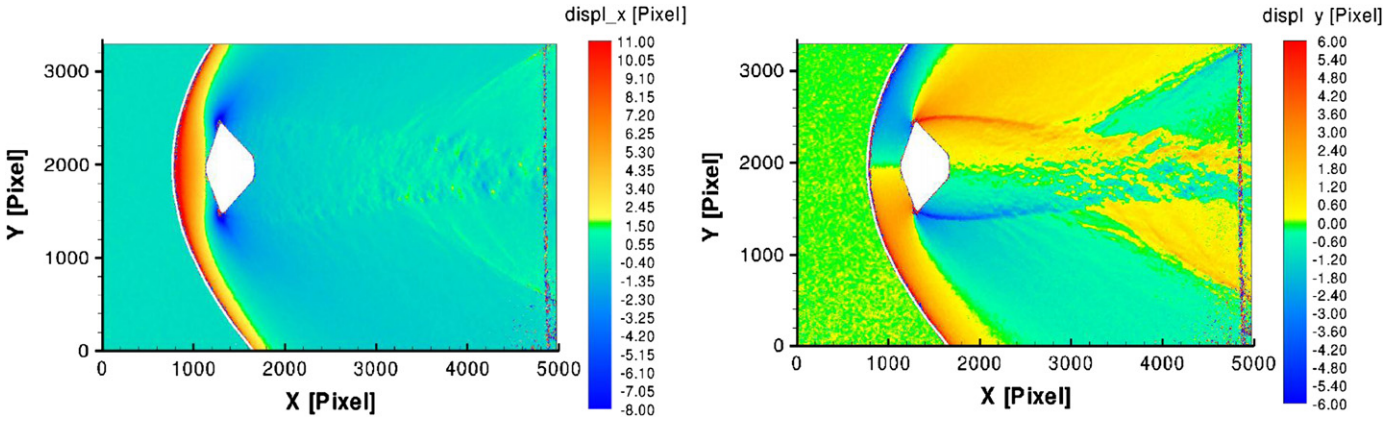

Fig. 27. Horizontal (left) and vertical (right) displacements of the rays through the flow around the model of the free flying space vehicle.

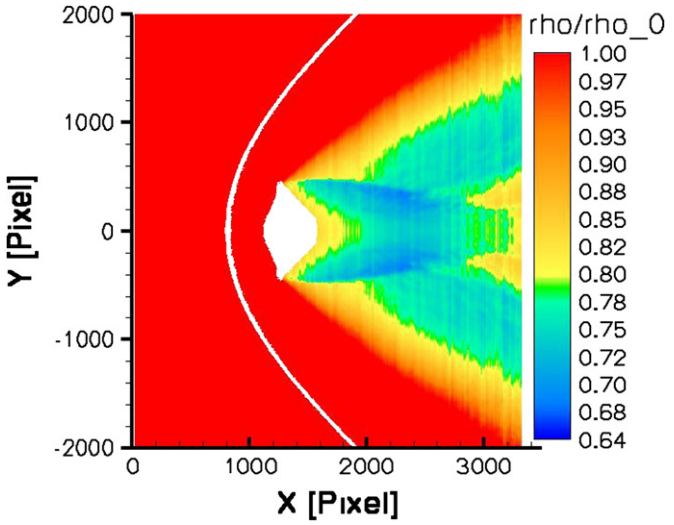

Fig. 28. Reconstruction of the density field from CBOS measurements.

In comparison with traditional methods, like the schlieren method, the differential interferometry, etc., the BOS technique is acknowledged for its simple optical setup and easy handling. In the case of the CBOS technique and due to the colored background, eight different dot patterns can be recorded simultaneously with one camera. Therefore, for every measurement eight correlations based on different dot patterns can be performed. The application of gliding interrogation windows allows us to increase the spatial resolution and the accuracy of the method. Furthermore, very large flow fields can be observed and even a landscape might be used as a background for this method.

Moreover, the accuracy and the spatial resolution of the CBOS technique allow to obtain a reliable reconstruction of the density field in complete steady three-dimensional flows in wind tunnel or around bodies in free-flight.

Acknowledgments

The authors wish to express their sincere thanks to J. Haertig, C. Berner and F. Jagusinski for their valuable help, comments and contributions.

References

[1] Settles GS. Schlieren and shadowgraph techniques. Berlin Heidelberg New York: Springer; 2001. p. 1–24.

[2] Desse JM, Deron R. Shadow, schlieren and color interferometry. ONERA J Aerosp Lab 2009(1):1–10.

[3] Debrus S, Francon M, Grover CP, May M, Robin ML. Ground glass differential interferometer. Appl Opt 1972;11:853.

[4] Köpf U. Application of speckling for measuring the deflection of laser light by phase objects. Opt Commun 1972;5:347–50.

[5] Wernekink U, Merzkirch W. Speckle photography of spatially extended refractive-index fields. Appl Opt 1987;26:31–2.

[6] Niessen R, Schäfer HJ, Merzkirch W. Measurement of length scales in the turbulent wake behind a cylindrical body at supersonic flow velocities. In: Proceedings of the IUTAM symposium on eddy structure identification in free turbulent shear flows, Poitiers, France, ISL-CO 235/92; 1992.

[7] Meier GEA. Hintergrund-Schlierenverfahren. Deutsche Patentanmeldung, DE 19942856A1; 1999.

[8] Raffel M. Optische Untersuchungen in technischen Strömungen unter besonderer Berücksichtigung eines Verfahrens zur Detektion von Dichtegradienten. Clausthal: Habilitationsschrift, Techn. Univ.; 2001.

[9] Richard H, Raffel M. Principle and applications of the Background Oriented Schlieren (BOS) method. Meas Sci Technol 2001;12(9):1576–85.

[10] Augenstein E, Leopold F, Richard H, Raffel, M. Schlieren techniques in comparison: Background Oriented Scattering versus visualization with holographic filters. In: Proceedings of the fourth International symposium on particle image velocimetry, Göttingen, DE, Paper 1191; 2001.

[11] Leopold F, Simon J, Gruppi, D, Schäfer HJ. Recent improvements of the Background Oriented Schlieren technique (BOS) using a colored background. In: Proceedings of the 12th International symposium on flow visualization, Göttingen, DE; 2006.

[12] Westerweel J. Digital particle image velocimetry, theory and application. Techn. Univ. Delft, Delft University Press; 1993.

[13] Klinge F, Riethmuller ML. Local density information obtained by means of the Background Oriented Schlieren (BOS) method. In: Proceedings of the 11th International symposium on application of laser techniques to fluid mechanics, Lisbon, Portugal; 2002.

[14] Hickel S. Entwicklung einer neuen echt dreidimensionalen Particle Image Velocimetry. Diplomarbeit BTU Cottbus; 2003.

[15] Sourgen F, Haertig J, Rey C. Comparison between Background Oriented Schlieren measurements (BOS) and numerical simulations. In: Proceedings of the 24th AIAA aerodynamic measurements technology and ground testing conference, Portland, USA; 2004.

[16] Kindler K, Goldhahn E, Leopold F, Raffel M. Recent developments in background oriented schlieren methods for rotor blade tip vortex measurements. Exp Fluids 2007;43:233–40.

[17] Grangeat P. La Tomographie. Hermes Lavoisier; 2002. ISBN 2-7462-0356-1.

[18] Kak CA, Slaney M. Principles of computerized tomographic imaging. IEEE Press; 1987. ISBN 0-87942-198-3.

[19] Shepp LA, Logan BF. The Fourier reconstruction of a head section. IEEE Trans Nucl Sci 1974;NS-21:21–43.